magnetism

MDPI

Article

Combined Molecular Dynamics and Micromagnetic Modelling of Nanocomposite Permanent Magnet Particle Arrangement and Properties

Nikolaos Maniotis [1,*], Nikolaos Vordos [2] and Michael Maragakis [2]

[1] Department of Physics, Aristotle University of Thessaloniki, 54124 Thessaloniki, Greece
[2] Department of Physics, Democritus University of Thrace, 65404 Kavala, Greece; nvordos@physics.duth.gr (N.V.); mmara@physics.duth.gr (M.M.)
* Correspondence: nimaniot@physics.auth.gr

Abstract

Nanocomposite rare-earth permanent magnets composed of exchange-coupled hard magnetic nanoparticles offer a promising route toward high-performance, rare-earth-efficient magnet technologies. In this work, we investigate the structural self-organization and magnetic hysteresis behavior of 40 nm $Sm_2Co_{17}/Nd_2Fe_{14}B$ hybrid nanoparticles using a combined molecular dynamics (MD) and micromagnetic simulation framework. First, MD simulations are employed to study the Brownian motion and field-induced assembly of the hybrid nanoparticles at two particle concentrations (1 and 5 mg/cm^3). In the absence of an external magnetic field, the nanoparticles display dispersed configurations governed by thermal fluctuations and interparticle interactions. Upon application of a high magnetic field (500 mT), the particles align into linear chain-like assemblies, with a more pronounced and rapid aggregation at higher concentration. Subsequently, micromagnetic calculations performed using the OOMMF are used to determine the magnetization reversal behavior of the assemblies. Quasi-static hysteresis loops at low field (40 mT) and room temperature reveal enhanced coercivity and remanence for field-aligned chain structures compared to randomly oriented particle ensembles. Additionally, increasing particle concentration amplifies the field-induced collective response due to stronger dipolar coupling. The combined MD–micromagnetic approach provides insight into structure–property relationships in magnetic nanocomposite systems and highlights the critical role of particle arrangement and concentration in determining magnet performance. These results contribute to the design principles for advanced nanostructured permanent magnets with tunable magnetic anisotropy and energy density.

Keywords: molecular dynamics; micromagnetics; nanocomposite permanent magnets; hysteresis loops; Tsallis q-statistics; dipolar interactions

Check for updates

Academic Editor: Łukasz Hawełek

Received: 4 June 2026
Revised: 4 July 2026
Accepted: 27 July 2026
Published: 4 August 2026

Copyright: © 2026 by the authors. Licensee MDPI, Basel, Switzerland. This article is an open access article distributed under the terms and conditions of the Creative Commons Attribution (CC BY) license.

1. Introduction

The ability to control the spatial arrangement of magnetic nanoparticles is a key factor in tailoring their collective magnetic response [1–3]. One particularly effective strategy involves directing nanoparticles into chain-like assemblies, a configuration known to substantially reinforce their magnetic behavior [4,5]. When magnetic particles align head-to-tail along an external field direction, magneto-dipolar coupling promotes cooperative magnetization processes, resulting in enhancements in key properties such as saturation magnetization, coercivity and effective anisotropy [6–9]. These improvements translate

directly into an increased hysteresis loop area, a parameter of critical importance for applications relying on high energy density, including next-generation permanent magnets and magnetic energy storage materials [10–12].

Depending on external and internal factors, magnetic nanoparticles can remain randomly dispersed or self-assemble into ordered structures [1,13]. Their spatial configuration is largely dictated by the interplay between magnetic dipolar interactions, thermal fluctuations, and the strength and direction of the applied magnetic field [14]. Whereas isolated, single-phase nanoparticles often form chain-like aggregates only under appropriate field conditions, hybrid or composite particles—consisting of two magnetically hard phases—exhibit more complex interaction landscapes [15,16]. In nanocomposites, the dipolar and exchange interactions between distinct magnetic phases can alter assembly behavior and modify the energy barriers governing particle orientation and chain formation [17,18]. Understanding these competing effects is therefore essential for designing nanostructures that take full advantage of cooperative magnetic phenomena.

Computational modeling provides a powerful route for analyzing nanoparticle arrangement at the nanoscale, where direct experimental characterization can be challenging [19]. Molecular dynamics (MD) simulations, in particular, allow for monitoring of particle motion and interactions under applied magnetic fields, enabling visualization of the transition from a dispersed state to field-induced chain configurations [20,21]. Experimental strategies to achieve similar structures typically involve dispersing nanoparticles in a viscoelastic or gel polymer matrix and applying high magnetic fields ($H > 0.1$ T), with viscosity, nanoparticle concentration, and temperature serving as key parameters controlling assembly kinetics and final morphology [22–25].

Despite significant progress in micromagnetic modeling of nanocomposite magnets, most studies assume idealized particle arrangements and therefore neglect the dynamic processes that govern nanoparticle assembly under external magnetic fields. In realistic systems, however, dipolar interactions, thermal fluctuations, and particle concentration determine the formation of chain-like structures that directly influence magnetic performance. Molecular dynamics simulations provide a powerful means to capture these assembly mechanisms, while micromagnetic simulations enable evaluation of the resulting hysteretic behavior and magnetic properties. The integration of these two approaches therefore bridges nanoscale structural evolution and macroscopic magnetic response, offering a predictive framework for the design of high-performance rare-earth nanocomposite magnets.

In the present study, we combine molecular dynamics and micromagnetic simulations to investigate the behavior of two-phase $Sm_2Co_{17}/Nd_2Fe_{14}B$ nanoparticles—materials known for their superior intrinsic magnetic performance and strong potential for high-energy permanent magnet applications [26,27]. These nanoparticles are not modeled as core–shell structures but rather as multi-phase nanocomposite particles where both magnetically hard phases coexist within the same nanoparticle volume. Such hybrid configurations are commonly employed in permanent magnet nanocomposites, where the coexistence of different hard magnetic phases may enhance magnetic performance through cooperative magnetization reversal and increased effective anisotropy. We initially track the motion and interactions of 40 nm hybrid nanoparticles dispersed in an agarose-like gel matrix under a static magnetic field of 500 mT, examining field-driven assembly into linear chains at two different particle concentrations. We then employ micromagnetic calculations using the Object-Oriented MicroMagnetic Framework (OOMMF) [28] to evaluate the resulting magnetic behavior, focusing on low-field hysteresis loop characteristics at room temperature for both random and field-oriented assemblies. A field amplitude of 0.04 T was selected to represent realistic operational conditions in low-field electromagnetic and permanent magnet-based applications [29,30]. In the micromagnetic simulations,

each nanoparticle is treated as an effective magnetic entity incorporating the intrinsic magnetic properties of both Sm_2Co_{17} and $Nd_2Fe_{14}B$ phases. The phases are assumed to be uniformly distributed within the nanoparticle volume, allowing the system to exhibit a composite magnetic response governed by exchange coupling, dipolar interactions, and external magnetic field effects. This approach enables the realistic modeling of hybrid nanocomposite particles while maintaining computational efficiency in the multiscale simulation framework. Through this multiscale computational approach, we elucidate the relationship between nanoscale structural organization and macroscopic magnetic properties in advanced nanocomposite magnet systems.

2. Materials and Methods

Under the assumption of micromagnetic theory, Brown [31] derived a set of equations after employing the magnetic Gibbs free energy, such as

$$E_t = \int (E_{ex} + E_a + E_z + E_d + E_{dip}) \tag{1}$$

In Equation (1), the total magnetic energy E_t is obtained by integrating over the entire volume of the ferromagnetic system. Each contribution reflects a distinct physical mechanism governing the magnetic behavior of the nanoparticles. The exchange energy E_{ex} represents the short-range interaction that aligns neighboring spins and favors uniform magnetization. The magnetocrystalline anisotropy term E_a captures the influence of the crystal lattice, and its magnitude and form depend on the symmetry of the material (e.g., uniaxial or cubic anisotropy). The Zeeman contribution E_z accounts for the interaction between the magnetic moments and an externally applied field H, tending to align the moments along the field direction. The demagnetizing or stray-field energy E_d arises from the dipolar field generated within the magnetic body itself and reflects the tendency of the system to minimize internal magnetic charges. Finally, the dipolar interaction term E_{dip} describes the long-range magnetostatic coupling between distinct nanoparticles, which plays a crucial role in collective behavior such as chaining, aggregation, and magnetically driven self-assembly. In the case of a magnetic nanocomposite consisting of N phases, the involved energies are given by the following expressions [32]:

$$E_{ex} = \sum_{i=1}^{N} A_i |\nabla \boldsymbol{M}_i|^2 V_i \tag{2}$$

$$E_a = \sum_{i=1}^{N} K_i V_i |\boldsymbol{M}_i|^2 \tag{3}$$

$$E_z = \sum_{i=1}^{N} \boldsymbol{M}_i V_i H \tag{4}$$

$$E_d = -\frac{\mu_0}{2} \sum_{i=1}^{N} \boldsymbol{M}_i \boldsymbol{H}_{di} V_i \tag{5}$$

$$E_{dip} = -\frac{1}{2} \sum_{i=1}^{N} \boldsymbol{M}_i \sum_{j \neq k}^{P} \frac{3\boldsymbol{e}_{jk}(\boldsymbol{e}_{jk}\boldsymbol{m}_{pj}) - \boldsymbol{m}_{pj}}{\Delta r_{jk}^3} \tag{6}$$

where A_i is the exchange stiffness constant, $\boldsymbol{M}_i$ the magnetization vector and $\boldsymbol{H}_{di}$ the demagnetizing field of the i-th phase. In Equation (6), P is the total number of nanocomposited particles, $\boldsymbol{m}_{pj}$ is the magnetization vector of the j-th particle and Δr_{jk} the distance between the j-th and k-th particles. Magnetization vectors of particles $\boldsymbol{m}_p$ are treated as point dipoles

located in the centers of generated closely packed spheres, while at the nanocomposite level, $\boldsymbol{M}_i$ is the total magnetization of individual phases.

From Equation (1), an effective magnetic field $\boldsymbol{H}_{eff}$ is derived, which incorporates all major contributions to the magnetic Gibbs free energy E. This effective field includes the externally applied field $\boldsymbol{H}$, the internal demagnetizing field $\boldsymbol{H}_{di}$, the long-range dipolar interactions, and the exchange field arising from short-range spin coupling. When a ferromagnetic system is subjected to an external magnetic stimulus, the local magnetization vector $\boldsymbol{M}_i$ responds to the presence of $\boldsymbol{H}_{eff}$, resulting in a time-dependent evolution of its orientation. The dynamic behavior of the magnetization under this combined effective field is rigorously described by the Landau–Lifshitz formalism, which governs the precessional motion and damping of magnetic moments toward equilibrium [33] and is expressed by the following equation:

$$\frac{d\boldsymbol{M_i}}{dt} = -\gamma \boldsymbol{M_i} \times \boldsymbol{H}_{eff} \tag{7}$$

The above relation governs the precessional motion of the magnetization vector $\boldsymbol{M}_i$ around the effective field $\boldsymbol{H}_{eff}$. However, magnetic hysteresis behavior demonstrates that above a certain threshold field, a ferromagnetic system reaches saturation, meaning that all magnetic moments eventually align with the applied field. Pure precessional motion cannot account for this irreversible alignment, since precession alone conserves energy and would not allow the system to settle into a fully aligned state [9,34]. Therefore, a mechanism for energy dissipation is required to describe the relaxation of magnetization toward equilibrium. To address this, Gilbert introduced a phenomenological damping term that represents the experimentally observable losses inherent in real magnetic materials. Incorporating this damping contribution leads to the well-known Landau–Lifshitz–Gilbert (LLG) equation, expressed as

$$\frac{d\boldsymbol{M_i}}{dt} = -\gamma \boldsymbol{M_i} \times \boldsymbol{H_{eff}} + \frac{\alpha}{M_s} \boldsymbol{M_i} \times \frac{d\boldsymbol{M_i}}{dt} \tag{8}$$

where α is the damping parameter and γ is the gyromagnetic ratio. The resulting dynamics from Equation (8) is a damped processional motion of magnetization vector $\boldsymbol{M_i}$, of each magnetic nanocomposite phase, around the effective field. Periodic boundary conditions were employed in the micromagnetic simulations. The collective influence of neighboring nanoparticles was introduced through an effective shape anisotropy obtained from the molecular dynamics simulations, whereas the demagnetization field computed by the OOMMF corresponds to the self-demagnetizing field of the simulated magnetic body.

The micromagnetic simulations were performed using material parameters obtained from the literature for Sm_2Co_{17} and $Nd_2Fe_{14}B$ at room temperature. The saturation magnetization (Ms), exchange stiffness constant (A), anisotropy constant (K_1), and Gilbert damping parameter (α) used in the simulations are summarized in Table 1. Both phases were considered to exhibit uniaxial magnetocrystalline anisotropy. These parameters were implemented within the OOMMF to simulate magnetization dynamics and hysteresis behavior of the hybrid nanocomposite particles.

Table 1. Micromagnetic parameters used in OOMMF simulations for Sm_2Co_{17} and $Nd_2Fe_{14}B$ phases at room temperature [35–38].

Material	Saturation Magnetization Ms (A/m)	Exchange Stiffness A (J/m)	Anisotropy Constant K_1 (J/m^3)	Damping Coefficient α	Easy Axis
Sm_2Co_{17}	8.0×10^5	1.0×10^{-11}	1.7×10^7	0.02	Uniaxial
$Nd_2Fe_{14}B$	1.27×10^6	7.7×10^{-12}	4.9×10^6	0.02	Uniaxial

Among all the energy terms contributing to the total magnetic energy in Equation (1), only two directly influence the translational motion of the nanoparticles in our system: the Zeeman energy E_z, associated with the externally applied static magnetic field, and the magneto-dipolar interaction energy E_{dip}, arising from interparticle magnetic coupling. These two contributions generate net forces capable of displacing the nanoparticles from their initial positions. As a result, particle motion is governed by the mechanical force $\boldsymbol{F}$, which can be expressed as

$$\boldsymbol{F} = -\boldsymbol{\nabla}\left(\boldsymbol{E_z} + \boldsymbol{E_{dip}}\right) \tag{9}$$

The nanoparticles are allowed to interact over a defined simulation window, enabling the observation of the system's temporal evolution and structural development. Their trajectories are obtained by numerically integrating Equation (9), in which the Zeeman energy E_z and the dipolar interaction energy E_{dip} are calculated using Equations (4) and (5), respectively. During the course of the simulation, the $Sm_2Co_{17}/Nd_2Fe_{14}B$ particles gradually organize into elongated chain-like structures, a process driven predominantly by the strong magnetostatic coupling under the applied magnetic field.

In the molecular dynamics simulations, nanoparticles were modeled as hybrid two-phase $Sm_2Co_{17}/Nd_2Fe_{14}B$ nanocomposite particles with a fixed diameter of 40 nm. Each particle was treated as a single spherical entity characterized by effective magnetic properties resulting from the coexistence of the hard magnetic Sm_2Co_{17} phase and the high-magnetization $Nd_2Fe_{14}B$ phase. This effective-particle approximation allows for the simulation of dipolar interactions and field-induced assembly without explicitly resolving the internal microstructure of each nanoparticle. The effective magnetic moment of each hybrid nanoparticle was calculated by considering the combined contribution of the two magnetic phases, weighted according to their volume fractions. In this way, all simulated particles maintain identical size and effective magnetic characteristics, consistent with the assumption of monodisperse hybrid nanocomposite nanoparticles. This approach is commonly employed in molecular dynamics simulations of magnetic nanocomposites, where the focus is placed on interparticle interactions and assembly behavior rather than internal phase distribution.

The computational procedure consists of two principal components. First, the translational and rotational motion of the particles is modeled through a Brownian dynamics framework [39], which accounts for thermal fluctuations and viscous resistance in the medium. Within this description, a particle cluster or chain composed of δ nanoparticles displays anisotropic diffusion behavior: motion parallel to the chain axis differs from motion perpendicular to it due to the elongated geometry and hydrodynamic constraints. This diffusion anisotropy plays a key role in the kinetics of chain growth and stabilization under applied magnetic fields. The diffusion coefficient for an isolated particle ($\delta = 1$) is

$$D_1 = \frac{k_B T}{3\pi\eta d_0} \tag{10}$$

where η is the viscosity of the gel matrix and d_0 the size of the particle. A chain for which $\delta \geq 2$ is characterized by a diffusion coefficient $D_\delta^{\parallel}$ in the direction parallel to the long axis of the growing chain and $D_\delta^{\perp}$ in the direction perpendicular to the long axis. The definition of these coefficients was possible through the following expressions adopted from slender body theory [40]:

$$\frac{D_\delta^{\parallel}}{D_1} = \frac{3}{2\delta}\left[\ln(2\delta) - \frac{1}{2}\right] \tag{11}$$

and

$$\frac{D_\delta^{\perp}}{D_1} = \frac{3}{2\delta}\left[\ln(2\delta) + \frac{1}{2}\right] \tag{12}$$

The second part is the dipolar interaction strength between nanoparticles expressed by Equation (6). The condition for chain formation is $E_{dip} \geq k_B T$ since the thermal kinetic energy $k_B T$ leads nanoparticles to random movements and attenuates the tendency for chain formation. Therefore, to promote restricted motion and reduce the effective degrees of freedom of the nanoparticles, the dipolar interaction energy between them must be comparable to or exceed the thermal energy. In practice, this criterion ensures that magnetic forces can overcome random Brownian agitation and drive cooperative organization. The molecular dynamics simulation begins from a thermally relaxed configuration in which $Sm_2Co_{17}/Nd_2Fe_{14}B$ nanoparticles are initially dispersed randomly within an agarose gel matrix. At this stage, all particles exist as isolated single units (i.e., $\delta = 1$, indicating the absence of chain structures), and each particle has a diameter of $d_0 = 40$ nm. This initial state represents a purely random dispersion prior to the onset of field-induced assembly and dipolar-driven interactions. The simulation is conducted for two concentrations, 1 and 5 mg/cm^3, within an 80 $d_0 \times 80\ d_0 \times 160\ d_0$ (nm^3) computational x, y, z space, respectively. The molecular dynamics simulations are intended to determine equilibrium nanoparticle configurations rather than to predict the experimental kinetics of chain formation. The physical assembly time depends on factors such as matrix viscosity, particle diffusivity and hydrodynamic interactions.

To evaluate the hysteresis behavior of the aligned nanoparticle assemblies, micromagnetic simulations were performed using the OOMMF software version 2.1 package. In the case of field-induced ordering, the chains of $Sm_2Co_{17}/Nd_2Fe_{14}B$ nanoparticles embedded in the agarose matrix are treated as elongated magnetic entities with an enhanced effective anisotropy. This additional anisotropy contribution originates from the chain geometry and is incorporated in the model as a uniaxial shape-anisotropy term. The "easy axis" of each chain is assumed to coincide with its longitudinal direction, reflecting the strong dipolar-induced alignment of the constituent particles.

By choosing $N = 2$ in Equations (2)–(6), the two magnetically hard rare-earth phases are effectively combined into a hybrid nanocomposite grain, allowing us to probe the collective response of the system. While qualitative trends regarding anisotropy enhancement and chain-driven magnetic behavior can be anticipated, the primary strength of the OOMMF approach lies in its ability to quantitatively compute the full hysteresis loop and extract key magnetic parameters. In particular, this method enables the evaluation of the relative changes in coercivity resulting from different nanoparticle arrangements and also the prediction of effective anisotropy and saturation magnetization as functions of phase composition and geometry, offering direct insight into the performance of the nanocomposite magnet.

The computational domain was discretized into cubic cells of $2 \times 2 \times 2$ nm^3, which is smaller than the characteristic exchange length of both Sm_2Co_{17} and $Nd_2Fe_{14}B$, ensuring accurate representation of magnetization variations. Each 40 nm nanoparticle was therefore discretized into multiple micromagnetic cells, allowing for spatially resolved magnetization dynamics within individual nanoparticles. The nanoparticle volumes were explicitly discretized and assigned magnetic material parameters corresponding to Sm_2Co_{17} and $Nd_2Fe_{14}B$ phases. The hybrid nanoparticles were modeled as two-phase nanocomposite structures with exchange coupling between adjacent cells. This approach allows for realistic simulation of magnetization reversal mechanisms, dipolar coupling, and collective magnetic behavior. The hybrid nanoparticle was modeled as a two-phase magnetic particle composed of equal volume fractions of Sm_2Co_{17} and $Nd_2Fe_{14}B$. Both phases were assumed to exhibit uniaxial magnetocrystalline anisotropy with a common easy axis. Prior to hysteresis calculations, the magnetization was initialized in the saturated state parallel to the applied magnetic field. The molecular dynamics simulations employed

a three-dimensional computational domain representing the agarose matrix, while the micromagnetic calculations were performed on discretized spherical nanoparticles using the $2 \times 2 \times 2\,nm^3$ computational cells. The number of MNPs was set equal to 200 and 1000 for the concentrations of 1 and 5 mg/mL, respectively.

Thermal fluctuations were also incorporated into the simulations to account for finite-temperature effects at room temperature (300 K). This was achieved by introducing a stochastic thermal field term (random noise field) in accordance with the fluctuation–dissipation theorem, ensuring a realistic representation of thermal agitation during magnetization dynamics [41]. The magnitude of the noise field is assumed to be the same in all three directions (isotropic), with a zero mean. Mathematically, these assumptions can be written as follows [41]: $\langle H_{th} \rangle = 0$, $\left\langle |H_{th}|^2 \right\rangle = \frac{2ak_BT}{\gamma MsV}$ and $\langle H_{th}(t)\, H_{th}(t+\tau) \rangle = \left\langle |H_{th}|^2 \right\rangle \delta(\tau)$. A crucial aspect of incorporating thermal fluctuations is the inherently time-dependent nature of the stochastic noise field. The amplitude of this thermal field scales with the temporal resolution of the simulation; in other words, the effective strength of the noise depends on the observation frequency. Consequently, the choice of numerical time step becomes a key parameter in ensuring physically meaningful magnetization dynamics. To accurately capture thermal effects while maintaining numerical stability, a constant integration time step of 3 ps was employed throughout the simulations. Additional test simulations were performed using smaller time steps (1–2 ps), and no significant variations in the resulting hysteresis loops or magnetization dynamics were observed. This confirms that the chosen time step ensures numerical stability, convergence of the stochastic thermal field implementation, and independence of the results from further time-step reduction. Simulations were continued until equilibrium was reached, defined by negligible variation in the total interaction energy and chain statistics during consecutive simulation steps.

It should be noted that different parameter treatments were employed in the molecular dynamics and micromagnetic simulation stages. The magnetic field applied during the molecular dynamics simulations, 500 mT, was used solely to promote field-assisted self-assembly and obtain equilibrium chain configurations. Subsequently, the micromagnetic simulations were performed using a lower magnetic field, 40 mT, to evaluate the influence of nanoparticle arrangement on low-field magnetization reversal. Therefore, the two field values correspond to different stages of the multiscale methodology and serve different physical objectives. Furthermore, in the molecular dynamics simulations, each $Sm_2Co_{17}/Nd_2Fe_{14}B$ nanoparticle was treated as an effective interacting entity characterized by a volume-averaged effective magnetic moment. In contrast, the micromagnetic simulations performed with the OOMMF did not use volume-averaged exchange stiffness or anisotropy parameters. Instead, the exchange stiffness constant (A) and magnetocrystalline anisotropy constant (K_1) were assigned locally at the discretization-cell level according to the corresponding magnetic phase, enabling spatially resolved simulation of magnetization dynamics within the hybrid nanoparticles.

3. Results and Discussion

In the simulations, an external magnetic field of 500 mT is applied along the z-axis. Under the influence of this field, the nanoparticles progressively interact, leading to aggregation and the emergence of elongated chain-like structures composed of an increasing number of particles. The simulation tracks the temporal evolution of these assemblies by monitoring the distribution of chains as a function of their length δ, defined as the number of nanoparticles within each chain. To illustrate the impact of the field, the spatial configurations of the nanoparticles are visualized both in the absence and presence of the applied magnetic field. These configurations are presented in Figure 1a,b, respectively, clearly demonstrating the transition from a random dispersion to a field-induced chain network.

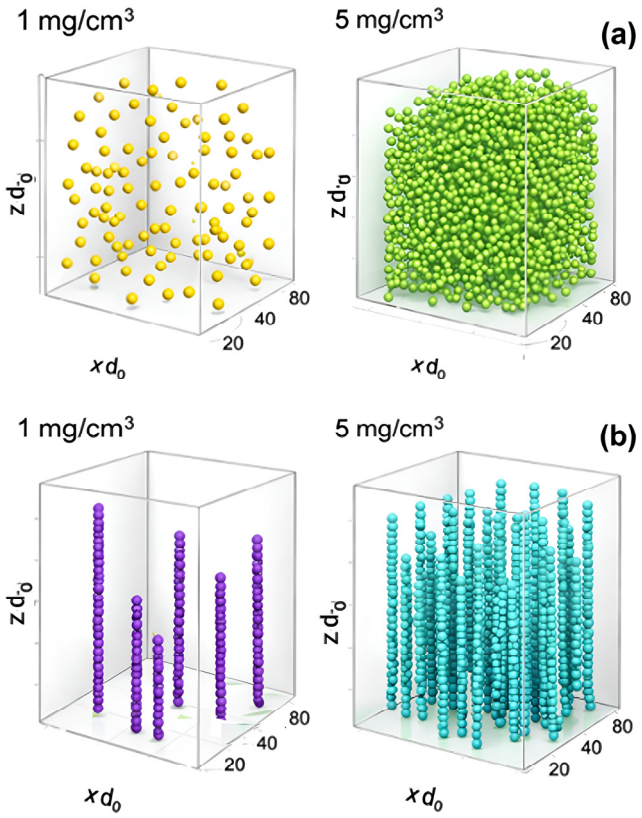


Figure 1. (**a**) Initial random spatial distribution of $Sm_2Co_{17}/Nd_2Fe_{14}B$ nanocomposite particles embedded in the agarose matrix in the absence of an external magnetic field, shown for two particle concentrations (1 and 5 mg/cm^3). (**b**) Field-induced assembly of nanoparticles into linear chains under a static magnetic field of 500 mT applied along the z-axis, for the same concentration values. The three-dimensional simulation volume, representing the gel matrix, has dimensions $x = y = 80d_0$ and $z = 160d_0$, where $d_0 = 40$ nm is the nanoparticle diameter.

In addition to magnetic dipolar interactions, short-range van der Waals forces may also contribute to nanoparticle aggregation. Previous studies have shown that magnetic dipolar interactions dominate the initial chain formation, while van der Waals forces mainly contribute to structural stabilization once nanoparticles approach small separations [42]. In the present system, the relatively large particle size (40 nm), high magnetic moment of $Sm_2Co_{17}/Nd_2Fe_{14}B$ phases, and the applied magnetic field favor dipolar-driven assembly. Consequently, van der Waals interactions are expected to play a secondary role, primarily stabilizing formed chains without significantly altering the dipolar-controlled assembly morphology. Therefore, although van der Waals forces are not explicitly included as a separate term in the MD force calculations, their physical role is implicitly reflected in the stabilization of the assembled structures and the resulting enhancement of collective magnetic behavior.

From Figure 1 it is clear that without the applied field, both systems remain in a dispersed state with no long-range order, as expected for magnetically hard nanoparticles embedded in a viscous gel-like environment. Thermal agitation dominates particle dynamics in this regime, preventing spontaneous large-scale aggregation despite the presence of dipolar coupling. However, subtle differences between the two concentrations are observed. At 5 mg/cm^3, particle–particle proximity increases significantly compared to the dilute system, leading to denser packing and more frequent local clustering. This behavior reflects the stronger contribution of dipolar interactions at higher concentrations, even under zero-field conditions, and highlights the tendency of hard-phase nanomagnets to experience non-negligible magnetic coupling at relatively short interparticle distances.

Upon application of the static magnetic field, shown in Figure 1b, the nanoparticle ensembles undergo a clear transition from random dispersions to elongated chain-like assemblies aligned parallel to the field direction. This transition is consistent with magnetically driven assembly mechanisms reported for single-phase magnetic nanoparticles, where dipolar interactions energetically favor head-to-tail alignment along the direction of magnetization. In the hybrid $Sm_2Co_{17}/Nd_2Fe_{14}B$ system, the strong intrinsic anisotropy and high coercivity of both phases enhance this behavior, leading to highly stable and well-defined chain structures. The particle arrangement in assembled structure is markedly more pronounced in the high-concentration case: the 5 mg/cm^3 suspension forms multiple long, closely spaced chains, whereas the lower-concentration system produces fewer chains with larger inter-chain separation. At higher nanoparticle concentration, the reduced average interparticle distance increases the strength of magnetic dipolar interactions, promoting the formation of more extended chain-like assemblies and larger interconnected aggregates at equilibrium. The present simulations characterize equilibrium morphologies rather than the long-term stability of the assembled structures. This observation underscores the cooperative nature of dipolar-driven assembly: as particle number density increases, the probability of dipolar capture and chain extension rises, yielding longer and more continuous structures. The formation of aligned magnetic chains has significant implications for macroscopic magnetic properties. Such ordered structures enhance interparticle magnetostatic coupling and reduce angular dispersion of magnetic moments relative to the field, both of which are favorable for strengthening coercivity and remanence. The simulation results therefore support the hypothesis that controlled field-induced assembly can be exploited as a processing route to tune the microstructure–property relationship in nanocomposite permanent magnets. Importantly, the use of a moderate field amplitude (0.04 T) demonstrates that chain formation can occur even under relatively low external stimuli, consistent with practical device environments. This finding is particularly relevant for nanocomposite magnet fabrication in polymer matrices or gel-assisted alignment processes, where high-field processing may be undesirable or energetically costly.

Furthermore, temperature plays a key role in determining nanoparticle assembly, as thermal energy competes with magneto-dipolar interactions. When the dipolar interaction energy exceeds the thermal energy k_BT, particle motion becomes increasingly constrained, promoting the formation of stable aggregates and linear chains. At room temperature, this competition is strongly influenced by particle concentration, since reduced interparticle distances enhance dipolar coupling. Consequently, higher concentrations favor interaction-dominated behavior, whereas dilute systems remain primarily governed by thermal fluctuations.

Magnetic hysteresis loops were computed using micromagnetic simulations at an applied field amplitude of 40 mT for both the chain-aligned and randomly dispersed nanoparticle systems at the two studied concentrations (1 and 5 mg/cm^3). For the oriented assemblies, the external magnetic field was applied along the easy axis—coincident with the chain alignment direction and parallel to the z-axis. In contrast, for the systems with randomly distributed nanoparticles, the applied field direction was varied randomly to reflect the absence of preferential orientation. The resulting hysteresis curves for all configurations are presented in Figure 2a. To further evaluate the influence of temperature on magnetization dynamics, additional zero-temperature micromagnetic simulations were performed for the chain-assembled $Sm_2Co_{17}/Nd_2Fe_{14}B$ nanoparticles at a concentration of 1 mg/cm^3. As shown in Figure 2b, the obtained hysteresis loop at 0 K exhibits sharper magnetization reversal and increased coercivity and magnetization compared to the 300 K case, reflecting the absence of thermally activated switching. In contrast, the 300 K loop displays smoother magnetization evolution and reduced coercive field due to thermal

fluctuations. Nevertheless, the overall enhancement associated with nanoparticle chain formation remains evident in both cases, confirming that dipolar-induced shape anisotropy dominates the magnetic response. These results demonstrate that temperature mainly affects switching smoothness and coercivity magnitude, without altering the fundamental chain-induced magnetic enhancement observed in the system.

It is evident that the hysteresis loops corresponding to the chain-aligned nanoparticles exhibit a noticeably larger area compared to those of the randomly oriented systems, independent of concentration. This demonstrates that the additional shape-anisotropy contribution arising from field-induced particle alignment strengthens the collective magnetic response, leading to an increased energy dissipation per cycle. In other words, the dipolar-driven formation of linear assemblies enhances the effective anisotropy and, consequently, the hysteresis loop area. In addition, the influence of particle concentration is clearly manifested in the magnetic behavior. Increasing the concentration reduces the mean interparticle spacing, which intensifies the magneto-dipolar interactions as indicated by Equation (6), and therefore increases the overall magnetic coupling within the system. Consistent with this expectation, the largest hysteresis loop area is observed for the aligned nanocomposite at the higher concentration of 5 mg/cm^3, confirming the cooperative effect of both chain formation and increased particle density on the macroscopic magnetic response. Note here that, although chain formation introduces shape anisotropy along the alignment direction, perfect easy-axis alignment of individual nanoparticles is not assumed. The coexistence of two magnetic phases, thermal fluctuations at room temperature, and magneto-dipolar interactions result in partial anisotropy dispersion and non-uniform magnetization configurations. Furthermore, the relatively low applied magnetic field used for hysteresis estimation may not fully saturate all particles. These factors collectively reduce the remanence-to-saturation ratio and explain the moderate magnetic anisotropy observed in the simulated hysteresis loops.

A quantitative comparison of the simulated magnetic properties further demonstrates the combined influence of nanoparticle concentration and field-induced chain formation on the magnetic response of the nanocomposite system. For the randomly distributed nanoparticles, increasing the concentration from 1 to 5 mg/cm^3 results in a noticeable enhancement in the magnetic properties due to the reduction in the average interparticle distance and the corresponding increase in dipolar interactions. Specifically, the coercive field increases by approximately 25%, while the remanent magnetization and saturation magnetization increase by about 20% and 10%, respectively. These changes indicate that even in the absence of field-assisted ordering, the closer proximity of neighboring nanoparticles strengthens the collective magnetic response through enhanced magnetostatic coupling. The effect becomes considerably more pronounced after field-induced assembly into linear chains. At a concentration of 1 mg/cm^3, chain formation increases the coercive field by approximately 75%, the remanent magnetization by about 37%, and the saturation magnetization by nearly 25% compared with the corresponding randomly distributed system. For the denser suspension (5 mg/cm^3), the effect is even stronger, with the coercivity increasing by approximately 80%, the remanence by about 36%, and the saturation magnetization by nearly 27%. In addition, the hysteresis loop area, which is directly related to the magnetic energy stored during one magnetization cycle, is estimated to increase by approximately 60% for the dilute sample and by nearly 70% for the concentrated sample following chain formation. These quantitative results clearly demonstrate that particle alignment contributes substantially beyond the concentration effect alone, confirming that the induced shape anisotropy associated with the linear chains promotes a more cooperative magnetization reversal process.

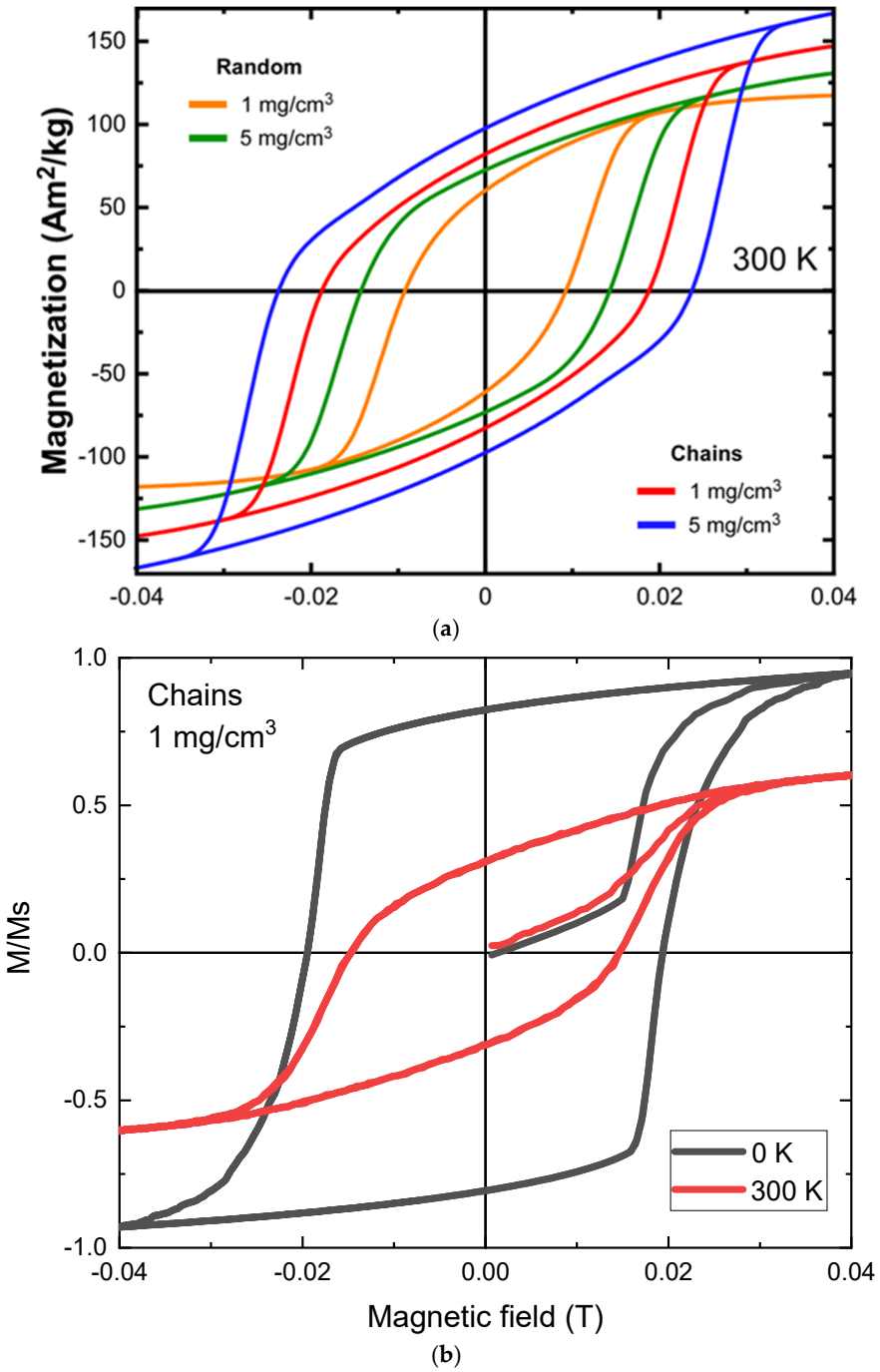


Figure 2. (**a**) Hysteresis loops simulated at an external field amplitude of 40 mT for 40 nm $Sm_2Co_{17}/Nd_2Fe_{14}B$ nanocomposite particles at 300 K. For the randomly distributed nanoparticles, the magnetic field direction was assigned randomly to reflect the absence of structural alignment. In the chain-aligned configuration, the external field was applied parallel to the chain axis, corresponding to the preferred (easy) magnetization direction of the assembled structure. (**b**) Temperature dependence of the magnetic hysteresis loops for linearly arranged nanoparticles at a concentration of 1 mg/cm^3. Micromagnetic simulations were performed at 0 K and 300 K with the external magnetic field applied along the chain alignment direction (*z*-axis). Magnetization values are normalized to the Ms value at 0 K. The 0 K loop exhibits sharper magnetization reversal and higher coercivity due to the absence of thermal activation, while the 300 K loop shows smoother switching behavior and reduced remanence magnetization resulting from thermally assisted magnetization dynamics.

The molecular dynamics simulations provide further evidence supporting this behavior. In the field-free configurations, nanoparticles remain randomly dispersed, whereas

under the applied assembly field they progressively organize into elongated chain-like structures oriented parallel to the magnetic field direction. Although nearly all nanoparticles participate in chain formation after equilibrium is reached, the extent of this participation depends on particle concentration. At the lower concentration (1 mg/cm^3), approximately 80–85% of the nanoparticles become incorporated into well-defined chains, while a small fraction remains isolated or forms only short aggregates because of the larger average interparticle separation. In contrast, at the higher concentration (5 mg/cm^3), approximately 95–98% of the nanoparticles participate in extended aligned structures, reflecting the much greater probability of dipolar capture between neighboring particles. This increase in particle participation is accompanied by a significant strengthening of the collective dipolar coupling. Since the magnetic dipole–dipole interaction energy varies inversely with the cube of the interparticle distance, even a moderate reduction in the average particle separation produces a disproportionately large increase in interaction strength. Consequently, the higher concentration facilitates stronger magnetic correlations, more efficient field-induced alignment, and improved collective ordering of the nanoparticle assembly. These structural changes provide the physical origin of the enhanced magnetic behavior observed in the micromagnetic simulations, linking the increased dipolar coupling and higher degree of particle alignment directly to the observed improvements in coercivity, remanence, saturation magnetization, and hysteresis loop area. Those results are summarized in Tables 2 and 3. The coercivity Hc, remanence Mr, saturation magnetization Ms, squareness ratio Mr/Ms, and normalized hysteresis loop area are reported for both randomly dispersed nanoparticles and field-induced linear chain assemblies at concentrations of 1 and 5 mg/cm^3, highlighting the enhancement of the magnetic response resulting from increased concentration and nanoparticle alignment.

Table 2. Estimated magnetic properties extracted from the simulated hysteresis loops.

Configuration	Hc (T)	Mr (Am^2/kg)	Ms (Am^2/kg)	Mr/Ms
Random, 1 mg/cm^3	0.012	60	118	0.51
Random, 5 mg/cm^3	0.015	72	130	0.55
Chains, 1 mg/cm^3	0.021	82	148	0.56
Chains, 5 mg/cm^3	0.027	98	165	0.59

Table 3. Quantitative comparison of the magnetic properties obtained from the micromagnetic simulations for 40 nm $Sm_2Co_{17}/Nd_2Fe_{14}B$ hybrid nanoparticles at 300 K.

Sample	ΔHc	ΔMr	ΔMs	Estimated Loop Area
Chains vs. Random (1 mg/cm^3)	+75%	+37%	+25%	+58%
Chains vs. Random (5 mg/cm^3)	+80%	+36%	+27%	+68%
Random (5 vs. 1 mg/cm^3)	+25%	+20%	+10%	+20%

While increasing nanoparticle concentration enhances dipolar coupling through reduced interparticle spacing, the formation of aligned chains introduces an additional contribution in the form of shape anisotropy. The elongated chain geometry creates a collective easy axis along the alignment direction, increasing the energy barrier for magnetization reversal. In randomly distributed systems, magnetic moments experience competing anisotropy directions, resulting in reduced cooperative switching. Consequently, chain alignment leads to enhanced coercivity, remanence, and hysteresis loop area beyond the effect of concentration alone.

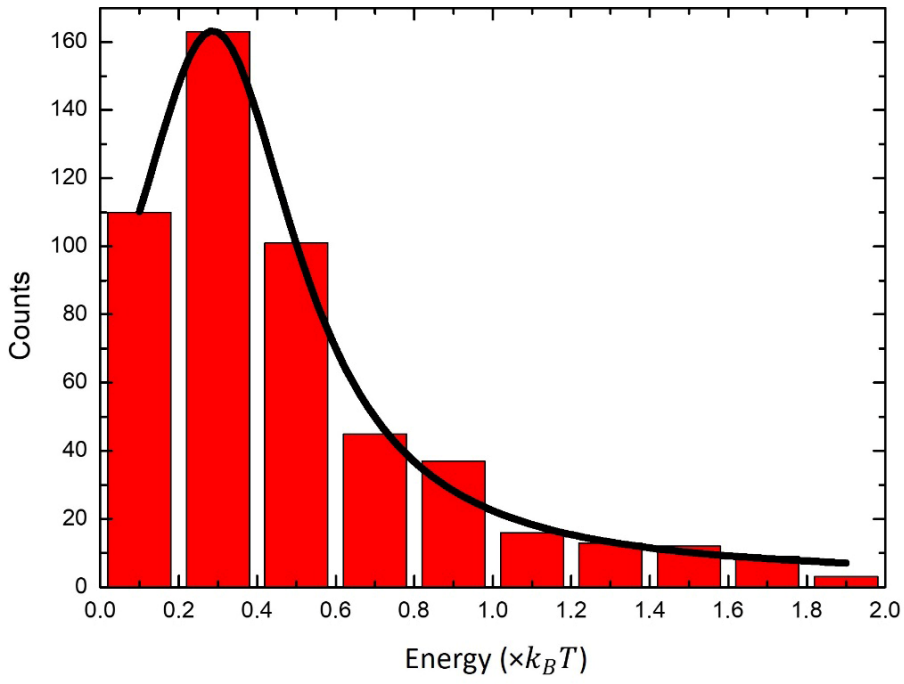
The coexistence of Sm_2Co_{17} and $Nd_2Fe_{14}B$ phases plays a key role in determining the magnetization reversal behavior due to their distinct intrinsic magnetic properties. Sm_2Co_{17}

is characterized by high magnetocrystalline anisotropy and large coercivity, acting as a magnetically hard phase that stabilizes magnetization against reversal. In contrast, $Nd_2Fe_{14}B$ exhibits high saturation magnetization and strong magnetic moment, contributing significantly to the overall magnetic response of the nanocomposite. When these two phases coexist within hybrid nanoparticles, exchange and magneto-dipolar interactions between the hard (Sm_2Co_{17}) and relatively softer ($Nd_2Fe_{14}B$) regions influence the magnetization reversal process. The hard phase acts as a pinning center that delays magnetization reversal, while the softer phase tends to reverse more easily under an applied field. This interplay leads to a more gradual and cooperative magnetization reversal mechanism, enhancing coercivity while maintaining high magnetization values. Furthermore, in chain-like arrangements, dipolar coupling between hybrid nanoparticles strengthens this cooperative behavior, as the aligned particles collectively resist reversal along the chain axis. This effect further increases the effective anisotropy and contributes to the enlargement of the hysteresis loop area observed in the micromagnetic simulations. Therefore, the coexistence of Sm_2Co_{17} and $Nd_2Fe_{14}B$ phases results in a favorable balance between high coercivity and high magnetization, which improves the overall magnetic performance of the nanocomposite system. Although comparison with single-phase Sm_2Co_{17} and $Nd_2Fe_{14}B$ nanoparticles would provide additional insight into the individual phase contributions to magnetization reversal, such an investigation falls beyond the scope of the present work, which focuses on the multiscale modeling of hybrid nanocomposite nanoparticles.

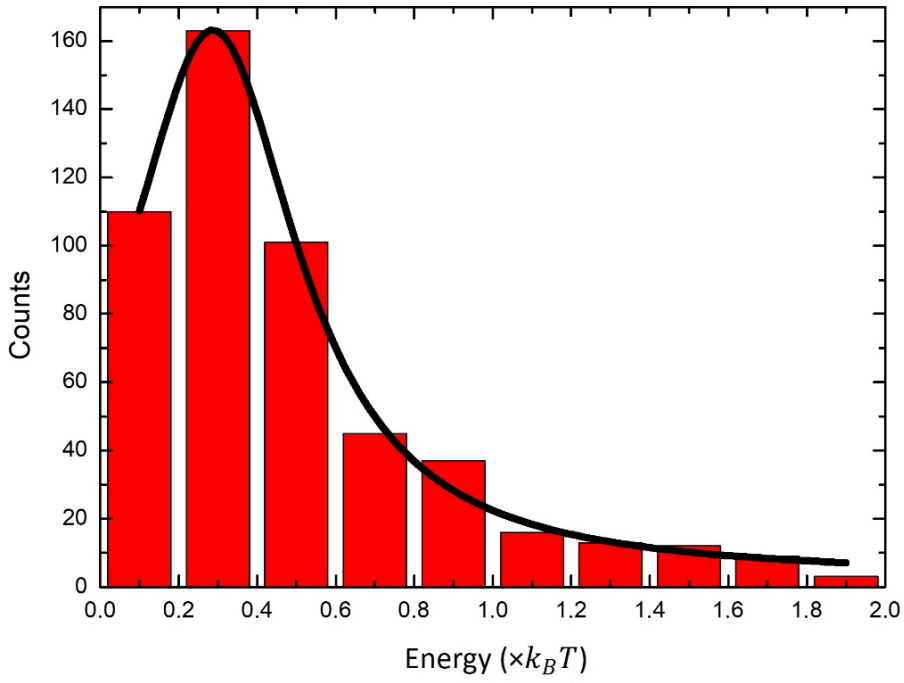
To further elucidate the effect of particle concentration and thermal fluctuations on the field-free behavior of the $Sm_2Co_{17}/Nd_2Fe_{14}B$ nanocomposite system, we analyzed the distribution of the total nanoparticle energy E_t obtained from the molecular dynamics simulations. The energy E_t includes all the aforementioned contributions except the Zeeman term, which is zero in the absence of a field, and is therefore dominated by dipolar interactions in this regime. Figure 3 shows the resulting energy histograms for the dilute (1 mg/cm^3) and dense (5 mg/cm^3) systems under zero applied field, together with the best-fit theoretical probability density curves.

In the dilute dispersion shown in Figure 3a, the majority of nanoparticles exhibit energies below k_BT, with only a small number exceeding this threshold and reaching values up to approximately 2 k_BT. This indicates that, at low concentration, thermal agitation dominates the particle dynamics, preventing large-scale aggregation. Nevertheless, the existence of a few particles with energies slightly above k_BT suggests the presence of transient small clusters or bead-like structures, which is consistent with the random-orientation morphology observed in Figure 1a. In the simulation code, the energetic criterion for chain stabilization is $E_d \geq k_BT$, reflecting that thermal motion must be overcome for magnetic dipolar alignment to persist. Thus, the dilute system is primarily governed by thermal disorder, and only rare, weakly bound pairs or small clusters form spontaneously without an external field.

A markedly different behavior emerges in the denser sample. As depicted in Figure 3b, only a minority of particles have energies below k_BT, while the vast majority lie above this level and extend to significantly higher energy values (up to ~12 k_BT). This energy distribution indicates that interparticle dipolar interactions become dominant as the concentration increases, promoting spontaneous aggregation and the formation of short chain-like structures even in the absence of an applied magnetic field. This behavior is consistent with the dense spatial configuration observed in Figure 1a, where the high number density enhances dipolar capture events and stabilizes interaction-mediated assemblies against thermal fluctuations.



(**a**)



(**b**)

Figure 3. (**a**) Probability distribution of the total nanoparticle energy E_t (normalized by k_BT) for the dilute sample (1 mg/cm^3) under zero applied magnetic field. Most particles exhibit energies below k_BT, indicating the dominance of thermal fluctuations and only sporadic formation of small clusters. The solid dark line represents the best-fit Tsallis q-Weibull distribution with $q = 1.3$ ($R^2 = 0.98$). After the fitting, the values of the dimensionless constants p_0 and r were both found to be equal to 1. (**b**) Probability distribution of total nanoparticle energy E_t (normalized by k_BT) for the dense system (5 mg/cm^3) without an applied magnetic field. The majority of particles possess energies above k_BT, demonstrating strong dipolar interactions and spontaneous formation of aggregates and short chains. The solid curve corresponds to the Tsallis q-Weibull fit with $q = 1.6$ ($R^2 = 0.99$). After the fitting, the values of the dimensionless constants p_0 and r were found to be equal to 1 and 1.5 respectively.

Upon applying a strong static magnetic field (500 mT), both systems evolve toward equilibrium configurations consisting of extended, well-aligned linear chains as shown in Figure 1b. In this oriented state, all particles reach nearly identical total energy values, indicating a uniform chain environment and confirming that the system has fully relaxed into a stable, field-aligned configuration. This ordered arrangement demonstrates the strong capability of the hybrid $Sm_2Co_{17}/Nd_2Fe_{14}B$ particles to respond collectively to an external field, even when Brownian contributions are present.

To quantitatively describe the energy distributions in the absence of field, we found that a Tsallis q-Weibull distribution, given by [43], was best fitted to the data. This probability density function (PDF) is given by the following equation:

$$p(E) = p_0 \frac{rE^{r-1}}{E_0^r} \left[1 - (1 - q)\left(\frac{E}{E_0}\right)^r\right]^{1/(1-q)} \quad (13)$$

In Equation (13), $p(E)$ is the energy probability density function, p_0 and r are dimensionless constants, E_0 is an energy constant that, in our case, equals a fraction of the thermal energy k_BT, and q is the Tsallis entropic index showing the deviation from extensivity. The so-called Tsallis Entropy [44] consists of a generalization of the Boltzmann–Gibbs entropy used for systems where long-range correlations are significant. When $q = 1$, the standard (extensive) Boltzmann entropy is recovered and the usual exponential factor (Boltzmann factor) describes equilibrium. But, if q differs from unity, the entropy becomes non-extensive (super-extensive for $q < 1$, and sub-extensive for $q > 1$), and the Boltzmann factor is generalized into a power-law. Usually q appears to reflect some (multi) fractality in the system. In magnetic nanoparticle systems, long-range dipolar interactions and aggregation processes introduce correlations between particles, leading to non-Gaussian energy distributions. Values of $q > 1$ indicate non-extensive behavior associated with cooperative interactions and clustering phenomena. The higher q value observed at increased concentration reflects stronger dipolar coupling and enhanced collective behaviour in the nanocomposite system.

Remarkably, excellent agreement was obtained in both samples ($R^2 = 0.98 - 0.99$), with non-extensivity parameters $q = 1.3$ for the dilute system and $q = 1.6$ for the dense one. For the first case, the values of $q > 1$ reveal the non-extensive and strongly interacting nature of the system, implying correlated particle dynamics and non-Gaussian statistics even in the zero-field (thermal) regime. The increase in q with concentration reflects the stronger interparticle coupling and collective behavior in the dense assembly, consistent with the higher observed dipolar energies and spontaneous clustering [45,46]. These results confirm that the $Sm_2Co_{17}/Nd_2Fe_{14}B$ nanocomposite suspension transitions from a weakly interacting thermal system at low concentration to a correlated dipolar fluid at high concentration, and that external magnetic fields can efficiently drive the system toward fully ordered, chain-like states with homogeneous energy distribution.

Equation (13) describes the probability density function of the total interaction energy within the nanoparticle ensemble at equilibrium. In practice, this energy is evaluated for each nanoparticle, considering its dipolar and Zeeman interactions with neighboring particles. Consequently, the distributions presented in Figure 3 correspond to the statistical distribution of particle-resolved interaction energies within the equilibrium ensemble. These distributions reflect the heterogeneity of interparticle interactions and the extent of aggregation within the system. Following the molecular dynamics simulations, the final equilibrium spatial configuration of nanoparticles was used as the input geometry for micromagnetic simulations. Thus, the hysteresis loops shown in Figure 2 correspond to the magnetic response of the equilibrium assemblies obtained from the MD simulations. In this manner, the statistical energy distributions derived from Equation (13) provide insight into

the interaction-driven assembly process, while the micromagnetic simulations evaluate the resulting magnetic properties of the formed structures.

The molecular dynamics results provide a microscopic foundation for interpreting the macroscopic magnetic behavior obtained from micromagnetic simulations. In particular, the spontaneous formation of small aggregates in the dilute system and extended dipolar-stabilized assemblies in the dense suspension—observed even in the absence of an external field—imply varying degrees of magnetic correlation dependent on particle concentration. These structural states directly influence magnetization reversal mechanisms. The OOMMF hysteresis loops confirm this relationship: randomly oriented ensembles show reduced remanence and lower coercivity, reflecting thermally induced misalignment and weak dipolar coupling. In contrast, the field-aligned chain configurations exhibit enhanced coercivity and remanent magnetization, consistent with cooperative dipolar coupling and suppressed thermal disorder as revealed in the MD simulations. Thus, the evolution from dispersed particles to ordered chain networks at higher concentration and under a field correlates with the transition from Brownian-dominated to interaction-dominated magnetic behavior, ultimately yielding improved magnet performance. The larger q value in the dense sample indicates a departure from classical Boltzmann–Gibbs behavior due to stronger dipolar frustration: in this regime, interparticle magnetic coupling generates correlated energy states and facilitates chain-formation energetics, revealing a collective, non-extensive character in the nanoparticle assembly.

Due to the complexity of magnetization behavior when nanoparticles are exposed to magnetic fields, only (relatively) simple problems of magnetization estimation can be solved analytically or numerically based on approximations such as the "macrospin" or "Double Well (DW)" models, which are valid for single-domain and single-phase magnetic nanoparticles [47–50]. These simplified approaches, however, inherently neglect several key ingredients governing the magnetization dynamics in multi-phase nanocomposite systems, including chain-mediated anisotropy, long-range dipolar coupling, and finite-temperature fluctuations. In contrast, the combined micromagnetic–molecular dynamics framework employed in this work captures the full spatial and temporal evolution of magnetization through a self-consistent effective field that incorporates exchange, anisotropy, Zeeman, magnetostatic and dipolar contributions. Furthermore, the statistical analysis of total energy fluctuations via Tsallis q-distributions reveals non-Gaussian behavior and non-extensive thermodynamics, particularly at higher nanoparticle concentrations where $q > 1$ evidences long-range correlations and interaction-driven collective states. This highlights that beyond realistic microstructural and magnetic field effects, non-extensive statistical behavior is a fundamental characteristic of interacting rare-earth nanomagnets, reinforcing the necessity of advanced simulation approaches that bridge many-body physics with mesoscale assembly dynamics.

It should also be noted here that the nanoparticles considered in the present work are dispersed within a non-magnetic agarose gel matrix at relatively low concentrations rather than forming a densely packed magnetic solid. Therefore, complete three-dimensional space filling is not physically expected in the modeled system. The nanoparticles were approximated as spherical particles with a diameter of 40 nm to simplify the multiscale simulations and isolate the effects of dipolar interactions and field-induced chain formation. In the micromagnetic simulations, the spherical geometry was discretized using cubic cells of $2 \times 2 \times 2$ nm^3 within the OOMMF. This discretization size is sufficiently small compared to the particle diameter and ensures accurate numerical representation of the spherical nanoparticle geometry and magnetization dynamics. Different nanoparticle morphologies may influence magnetic behavior through variations in shape anisotropy, demagnetizing fields, and interparticle coupling strength. For example, cubic or elongated

nanoparticles may exhibit enhanced anisotropy and modified magnetization reversal mechanisms compared to spherical particles. However, a systematic investigation of morphology-dependent effects is beyond the scope of the present study and may constitute an interesting direction for future work.

Although the present study considers two representative nanoparticle concentrations, the observed trends indicate a more general concentration-dependent evolution of the assembly process. As the particle concentration increases, the average interparticle distance decreases, leading to stronger dipolar interactions that progressively favor the transition from isolated particles and small aggregates toward extended chain-like structures. Consequently, a critical concentration is expected to exist at which collective magnetic interactions become sufficiently strong to promote the formation of a percolating network of aligned chains. Determining this transition concentration would require a systematic investigation over a wide range of concentrations together with statistical analysis of multiple equilibrium configurations, which is beyond the scope of the present work. Nevertheless, the combined molecular dynamics–micromagnetic framework presented here provides a suitable computational platform for such investigations and could assist in establishing concentration design criteria for the optimization of nanocomposite permanent magnets in future studies.

4. Conclusions

The combined molecular dynamics and micromagnetic simulations presented in this work reveal how nanoparticle concentration and magnetic field-assisted assembly jointly dictate the structural and magnetic behavior of $Sm_2Co_{17}/Nd_2Fe_{14}B$ nanocomposites. Molecular dynamics results demonstrate that dipolar interactions, when sufficiently strong relative to thermal energy, drive the formation of linear nanoparticle chains under an applied magnetic field. At low particle concentration, chain growth is limited by reduced collision probability, producing isolated short chains. Increasing the concentration significantly enhances dipolar coupling, enabling the formation of longer, more stable chain networks with high alignment fidelity. These microstructural transitions are reflected in the macroscopic magnetic response: micromagnetic simulations show that chain alignment results in a substantially larger hysteresis loop area compared to randomly dispersed nanoparticles, with the highest magnetic performance obtained for the dense, field-aligned configuration. This enhancement is attributed to the effective anisotropy introduced by the elongated chain geometry, which acts as a collective "easy axis" and strengthens the cooperative magnetic response.

A key outcome of this study is the identification of non-Gaussian energy statistics in the nanoparticle ensembles prior to field alignment. By fitting the total energy distributions to a Tsallis q-Weibull function, we find $q = 1.3$ for the dilute dispersion and $q = 1.6$ for the higher-concentration case. These $q > 1$ values unambiguously indicate non-extensive statistical behavior, reflecting long-range dipolar coupling, aggregation tendencies even in the absence of external fields, and a departure from simple thermal equilibrium. The systematically larger q in the denser system confirms stronger collective interactions and a more correlated energy landscape. These observations establish Tsallis non-extensive statistics as a powerful diagnostic tool for quantifying magnetic interaction strength and the onset of self-organization in nanocomposite magnet systems.

Taken together, the results highlight the importance of integrating molecular dynamics with micromagnetic simulation to accurately capture both the nanoscale assembly dynamics and the emergent macroscopic magnetic behavior. This multiscale computational framework provides predictive insight into the design of high-performance nanocomposite permanent magnets, enabling rational tuning of particle concentration, microstructural

arrangement, and processing fields. As advanced rare-earth nanocomposites continue to evolve, such hybrid simulation methodologies will play a central role in guiding materials engineering strategies, accelerating experimental development, and optimizing energy-dense magnetic systems beyond what can be achieved through trial-and-error experimentation alone.

Author Contributions: Conceptualization, N.M., N.V. and M.M.; methodology, N.M., N.V. and M.M.; software, N.M., N.V. and M.M.; validation, N.M., N.V. and M.M.; formal analysis, N.M., N.V. and M.M.; investigation, N.M., N.V. and M.M.; resources, N.M., N.V. and M.M.; data curation, N.M., N.V. and M.M.; writing—original draft preparation, N.M., N.V. and M.M.; writing—review and editing, N.M., N.V. and M.M.; visualization, N.M., N.V. and M.M.; supervision, N.M., N.V. and M.M.; project administration, N.M., N.V. and M.M. All authors have read and agreed to the published version of the manuscript.

Funding: This research received no external funding.

Institutional Review Board Statement: Not applicable.

Informed Consent Statement: Not applicable.

Data Availability Statement: The raw data supporting the conclusions of this article will be made available by the authors on request.

Conflicts of Interest: The authors declare no conflicts of interest.

References

1. Gu, H.; Chen, Y.; Lüders, A.; Bertrand, T.; Hanedan, E.; Nielaba, P.; Bechinger, C.; Nelson, B.J. Scalable high-throughput microfluidic separation of magnetic microparticles. *Device* **2024**, *2*, 100403. [CrossRef] [PubMed]
2. Saville, S.L.; Qi, B.; Baker, J.; Stone, R.; Camley, R.E.; Livesey, K.L.; Ye, L.; Crawford, T.M.; Mefford, O.T. The formation of linear aggregates in magnetic hyperthermia: Implications on specific absorption rate and magnetic anisotropy. *J. Colloid Interface Sci.* **2014**, *424*, 141–151. [CrossRef] [PubMed]
3. Gavilán, H.; Simeonidis, K.; Myrovali, E.; Mazarío, E.; Chubykalo-Fesenko, O.; Chantrell, R.; Balcells, L.; Angelakeris, M.; Morales, M.P.; Serantes, D. How size, shape and assembly of magnetic nanoparticles give rise to different hyperthermia scenarios. *Nanoscale* **2021**, *13*, 15631–15646. [CrossRef] [PubMed]
4. Chen, H.; Billington, D.; Riordan, E.; Blomgren, J.; Giblin, S.R.; Johansson, C.; Majetich, S.A. Tuning the dynamics in Fe_3O_4 nanoparticles for hyperthermia optimization. *Appl. Phys. Lett.* **2020**, *117*, 073702. [CrossRef]
5. Myrovali, E.; Maniotis, N.; Makridis, A.; Terzopoulou, A.; Ntomprougkidis, V.; Simeonidis, K.; Sakellari, D.; Kalogirou, O.; Samaras, T.; Salikhov, R.; et al. Arrangement at the nanoscale: Effect on magnetic particle hyperthermia. *Sci. Rep.* **2016**, *6*, 37934. [CrossRef] [PubMed]
6. Ovejero, J.G.; Cabrera, D.; Carrey, J.; Valdivielso, T.; Salas, G.; Teran, F.J. Effects of inter- and intra-aggregate magnetic dipolar interactions on the magnetic heating efficiency of iron oxide nanoparticles. *Phys. Chem. Chem. Phys.* **2016**, *18*, 10954–10963. [CrossRef] [PubMed]
7. Maniotis, N.; Nazlidis, A.; Myrovali, E.; Makridis, A.; Angelakeris, M.; Samaras, T. Estimating the effective anisotropy of ferromagnetic nanoparticles through magnetic and calorimetric simulations. *J. Appl. Phys.* **2019**, *125*, 103903. [CrossRef]
8. Ali, Q.; Fischbacher, J.; Kovacs, A.; Oezelt, H.; Gusenbauer, M.; Moustafa, H.; Böhm, D.; Breth, L.; Schrefl, T. Defect manipulation for the coercivity enhancement of Nd-Fe-B permanent magnets. *Phys. B Condens. Matter* **2024**, *678*, 415759. [CrossRef]
9. Jalal, E.M.; Saadi, H.; Hasnaoui, A.; Hachem, O.; Lafhal, A.; Madani, M.; El Bouziani, M. Single-Ion Anisotropy Effect on the Critical and Hysteresis Behaviors of a Mixed-Spin (1, 3/2) Square Ising Nanowire. *Phys. Status Solidi Basic Res.* **2023**, *260*, 2300180. [CrossRef]
10. El-Gendy, A.A.; Barandiarán, J.M.; Hadimani, R.L. (Eds.) Magnetic Nanostructured Materials: From Lab to Fab. In *Magnetic Nanostructured Materials*; Elsevier: Amsterdam, The Netherlands, 2018. [CrossRef]
11. Eklund, P.; Eriksson, S. Air gap magnetic flux density variations due to manufacturing tolerances in a permanent magnet synchronous generator. In *Proceedings of the 2016 22nd International Conference on Electrical Machines (ICEM), Lausanne, Switzerland, 4–7 September 2016*; IEEE: New York, NY, USA, 2016; pp. 93–99. [CrossRef]
12. Perin, D.; Dogru, M.B.; Gonen Ocaktan, D.; Oral, A.; Karaoglan, A.D. Magnetic Flux Density Distribution of 1.5 kW Permanent Magnet Synchronous Generator by using Response Surface Methodology. In Proceedings of the 7th World Congress on Mechanical, Chemical, and Material Engineering (MCM'21), Virtual Event, 2–4 August 2021. [CrossRef]

13. Andreu, J.S.; Camacho, J.; Faraudo, J. Aggregation of superparamagnetic colloids in magnetic fields: The quest for the equilibrium state. *Soft Matter* **2011**, *7*, 2336–2339. [CrossRef]
14. Maniotis, N.; Kalaitzidou, K.; Asimoulas, E.; Simeonidis, K. A rotary magnetic separator integrating nanoparticle-assisted water purification: Simulation and laboratory validation. *J. Water Process Eng.* **2023**, *53*, 103825. [CrossRef]
15. Ahsan, M.A.; Jabbari, V.; Imam, M.A.; Castro, E.; Kim, H.; Curry, M.L.; Valles-Rosales, D.J.; Noveron, J.C. Nanoscale nickel metal organic framework decorated over graphene oxide and carbon nanotubes for water remediation. *Sci. Total Environ.* **2020**, *698*, 134214. [CrossRef] [PubMed]
16. Kaewsaneha, C.; Tangboriboonrat, P.; Polpanich, D.; Elaissari, A. Multifunctional Fluorescent-Magnetic Polymeric Colloidal Particles: Preparations and Bioanalytical Applications. *ACS Appl. Mater. Interfaces* **2015**, *7*, 23373–23386. [CrossRef] [PubMed]
17. Liu, X.; Zhong, W.; Gu, B.; Du, Y. Exchange-coupling interaction in nanocomposite $SrFe_{12}O_{19}/\gamma$-Fe_2O_3 permanent ferrites. *J. Appl. Phys.* **2002**, *92*, 1028–1032. [CrossRef]
18. Das, A.; Mohanty, S.; Kumar, R.; Kuanr, B.K. Tailoring the Design of a Lanthanide Complex/Magnetic Ferrite Nanocomposite for Efficient Photoluminescence and Magnetic Hyperthermia Performance. *ACS Appl. Mater. Interfaces* **2020**, *12*, 42016–42029. [CrossRef] [PubMed]
19. Zhigilei, L.V.; Volkov, A.N.; Dongare, A.M. Computational Study of Nanomaterials: From Large-Scale Atomistic Simulations to Mesoscopic Modeling. In *Encyclopedia of Nanotechnology*; Springer: Dordrecht, The Netherlands, 2016. [CrossRef]
20. Vogiatzis, G.G.; Theodorou, D.N. Multiscale Molecular Simulations of Polymer-Matrix Nanocomposites: Or What Molecular Simulations Have Taught us About the Fascinating Nanoworld. *Arch. Comput. Methods Eng.* **2018**, *25*, 591–645. [CrossRef] [PubMed]
21. Golovin, Y.I.; Gribanovsky, S.L.; Golovin, D.Y.; Zhigachev, A.O.; Klyachko, N.L.; Majouga, A.G.; Sokolsky, M.; Kabanov, A.V. The dynamics of magnetic nanoparticles exposed to non-heating alternating magnetic field in biochemical applications: Theoretical study. *J. Nanopart. Res.* **2017**, *19*, 59. [CrossRef]
22. Fragouli, D.; Torre, B.; Bertoni, G.; Buonsanti, R.; Cingolani, R.; Athanassiou, A. Formation and microscopic investigation of iron oxide aligned nanowires into polymeric nanocomposite films. *Microsc. Res. Tech.* **2010**, *73*, 952–958. [CrossRef] [PubMed]
23. Myrovali, E.; Maniotis, N.; Samaras, T.; Angelakeris, M. Spatial focusing of magnetic particle hyperthermia. *Nanoscale Adv.* **2020**, *2*, 408–416. [CrossRef] [PubMed]
24. Skumiel, A.; Kaczmarek, K.; Flak, D.; Rajnak, M.; Antal, I.; Brząkała, H. The influence of magnetic nanoparticle concentration with dextran polymers in agar gel on heating efficiency in magnetic hyperthermia. *J. Mol. Liq.* **2020**, *304*, 112734. [CrossRef]
25. Javidi, M.; Heydari, M.; Attar, M.M.; Haghpanahi, M.; Karimi, A.; Navidbakhsh, M.; Amanpour, S. Cylindrical agar gel with fluid flow subjected to an alternating magnetic field during hyperthermia. *Int. J. Hyperth.* **2015**, *31*, 33–39. [CrossRef] [PubMed]
26. Yin, X.; Sui, Y.; Yang, Q.; Shen, Q.; Ma, Y.; Shao, B.; Sun, J.; Guo, D. Preparation and magnetic properties of anisotropic $Nd_2Fe_{14}B/Sm_2Co_{17}$ hybrid-bonded magnets. *J. Rare Earths* **2019**, *37*, 1047–1052. [CrossRef]
27. An, S.; Ma, Z.; Li, W.; Zhang, H.; Yin, T. Magnetic properties of anisotropic bonded NdFeB/SmCo permanent magnets. *AIP Adv.* **2019**, *9*, 125146. [CrossRef]
28. Donahue, M.J.; Porter, D.G. *OOMMF User's Guide*; Version 1.0; U.S. Department of Commerce: Gaithersburg, MD, USA, 1999. [CrossRef]
29. Yamaji, K.; Shimonosono, T.; Kishimoto, H.; Togawa, M.; Fujii, S.; Imura, M.; Tamura, C.; Hayashi, T.; Kikuchi, Y.; Hirosawa, S.; et al. Miyashita, Perspectives for high-performance permanent magnets: Applications, coercivity, and new materials*. *Adv. Nat. Sci. Nanosci. Nanotechnol.* **2017**, *8*, 013002. [CrossRef]
30. He, T.; Zhu, Z.; Eastham, F.; Wang, Y.; Bin, H.; Wu, D.; Gong, L.; Chen, J. Permanent Magnet Machines for High-Speed Applications. *World Electr. Veh. J.* **2022**, *13*, 18. [CrossRef]
31. Brown, W. *Micromagnetics*; Interscience Publishers: New York, NY, USA; London, UK, 1963.
32. Maniotis, N.; Simeonidis, K. Analytical Approaches of Magnetic Hybrid Nanoparticles Using Numerical Modelling and Simulation Tools. In *Handbook of Magnetic Hybrid Nanoalloys and Their Nanocomposites*; Springer: Cham, Switzerland, 2022. [CrossRef]
33. Mahalingam, S.S.; Manikandan, B.V.; Arockiaraj, S. Review—Micromagnetic Simulation Using OOMMF and Experimental Investigations on Nano Composite Magnets. *J. Phys. Conf. Ser.* **2019**, *1172*, 012070. [CrossRef]
34. Lafhal, A.; Jalal, E.M.; Hasnaoui, A.; Saadi, H.; Hachem, N.; Madani, M.; El Bouziani, M. Magnetic Behavior of Ising Nanowire with Mixed Integer Spins: A Monte Carlo Study. *J. Nano Res.* **2023**, *77*, 155–168. [CrossRef]
35. Kronmüller, H.; Fähnle, M. *Micromagnetism and the Microstructure of Ferromagnetic Solids*; Cambridge University Press: Cambridge, UK, 2003; 432p. Available online: https://books.google.com/books/about/Micromagnetism_and_the_Microstructure_of.html?hl=el&id=h6nKtwcYyNEC (accessed on 3 May 2026).
36. Skomski, R.; Coey, J.M.D. *Permanent Magnetism*, 1st ed.; Routledge: Abingdon, UK, 1999. Available online: https://www.routledge.com/Permanent-Magnetism/Skomski-Coey/p/book/9780750304788 (accessed on 3 May 2026).
37. Coey, J.M.D. (Ed.) *Rare-Earth Iron Permanent Magnets*; Oxford University Press: Oxford, UK, 1996. [CrossRef]

38. Gutfleisch, O.; Willard, M.A.; Brück, E.; Chen, C.H.; Sankar, S.G.; Liu, J.P. Magnetic materials and devices for the 21st century: Stronger, lighter, and more energy efficient. *Adv. Mater.* **2011**, *23*, 821–842. [CrossRef] [PubMed]
39. Andreu, J.S.; Calero, C.; Camacho, J.; Faraudo, J. On-the-fly coarse-graining methodology for the simulation of chain formation of superparamagnetic colloids in strong magnetic fields. *Phys. Rev. E Stat. Nonlinear Soft Matter Phys.* **2012**, *85*, 036709. [CrossRef] [PubMed]
40. Brenner, H. Stokes wall effects for particles moving near cylindrical boundaries. *J. Fluid Mech.* **1985**, *154*, 145–162. [CrossRef]
41. Schrefl, T.; Fidler, J.; Suess, D.; Scholz, W.; Tsiantos, V. Micromagnetic Simulation of Dynamic and Thermal Effects. In *Handbook of Advanced Magnetic Materials*; Springer: Boston, MA, USA, 2006; pp. 128–146. Available online: https://www.academia.edu/4133829/Micromagnetic_Simulation_of_Dynamic_and_Thermal_Effects (accessed on 8 February 2023).
42. Bian, B.; Chen, G.; Zheng, Q.; Du, J.; Lu, H.; Liu, J.P.; Hu, Y.; Zhang, Z. Self-Assembly of CoPt Magnetic Nanoparticle Arrays and its Underlying Forces. *Small* **2018**, *14*, 1801184. [CrossRef] [PubMed]
43. Tsallis, C. *Introduction to Nonextensive Statistical Mechanics: Approaching a Complex World*; Springer: New York, NY, USA, 2009; pp. 1–382. [CrossRef]
44. Tsallis, C. Possible generalization of Boltzmann-Gibbs statistics. *J. Stat. Phys.* **1988**, *52*, 479–487. [CrossRef]
45. Guisbiers, G. Advances in thermodynamic modelling of nanoparticles. *Adv. Phys. X* **2019**, *4*, 1668299. [CrossRef]
46. Maniotis, N.; Frangis, N. The connection between Hill's nanothermodynamics and Tsallis non-extensive statistical mechanics: Extracting the thermodynamic properties of a nanosystem. *Phys. E Low Dimens. Syst. Nanostruct.* **2025**, *172*, 116285. [CrossRef]
47. Carrey, J.; Mehdaoui, B.; Respaud, M. Simple models for dynamic hysteresis loop calculations: Application to hyperthermia optimization Abstract. *J. Appl. Phys.* **2011**, *109*, 083921. [CrossRef]
48. Allia, P.; Barrera, G.; Tiberto, P. Nonharmonic Driving Fields for Enhancement of Nanoparticle Heating Efficiency in Magnetic Hyperthermia. *Phys. Rev. Appl.* **2019**, *12*, 034041. [CrossRef]
49. Roda-Llordes, M.; Riera-Campeny, A.; Candoli, D.; Grochowski, P.T.; Romero-Isart, O. Macroscopic Quantum Superpositions via Dynamics in a Wide Double-Well Potential. *Phys. Rev. Lett.* **2024**, *132*, 023601. [CrossRef] [PubMed]
50. Serantes, D. Superparamagnetism and Monte Carlo Simulations. *Open Surf. Sci. J.* **2012**, *4*, 71–84. [CrossRef]

Disclaimer/Publisher's Note: The statements, opinions and data contained in all publications are solely those of the individual author(s) and contributor(s) and not of MDPI and/or the editor(s). MDPI and/or the editor(s) disclaim responsibility for any injury to people or property resulting from any ideas, methods, instructions or products referred to in the content.